CrossMark

ORIGINAL PAPER

A fast green synthesis of Ag nanoparticles in carboxymethyl cellulose (CMC) through UV irradiation technique for antibacterial applications

Mohamed Basuny[1] · Ibraheem O. Ali[1] · Ahmed Abd El-Gawad[2] · Mostafa F. Bakr[1] · Tarek M. Salama[1]

Abstract Silver nanoparticles embedded in a carboxymethyl cellulose matrix (AgNPs/CMC) were synthesized by a UV irradiation technique. The successful formation of AgNPs/CMC was examined using UV–Vis spectroscopy, XPS, XRD, TEM, and FTIR. The factors in the preparation process that affected the final products were extensively studied. Thus, 5.0 mM AgNO$_3$, 0.5 g l^{-1} CMC, and exposure to UV light for 2.5 min provide excellent combinations to accomplish the AgNPs/CMC formation. Measurements of optical spectra showed that the surface plasmon resonance was localized around 426 nm when the reaction mixture exposed to UV light for 0.5 min; that is monotonically blue shifted to 403 nm up to 2.5 min exposure time. This is manifested in a quick reduction of Ag$^+$ into smaller Ag nanoparticles. The IR analysis indicated that hydroxyl and carboxylate groups in CMC were included in coordination with the Ag$^+$ ions through displacement of one proton. Upon absorbing UV light, the cellulose hydroxyl and carboxymethylic groups get excited, which reduce Ag$^+$ ions to Ag nanoparticles. The TEM image for the optimal designed AgNPs/CMC sample confirmed that AgNPs are formed with many individual spherical shapes and an average diameter of 15.5 nm. This AgNPs/CMC sample showed promising antibacterial properties toward *E. coli*.

Graphical Abstract
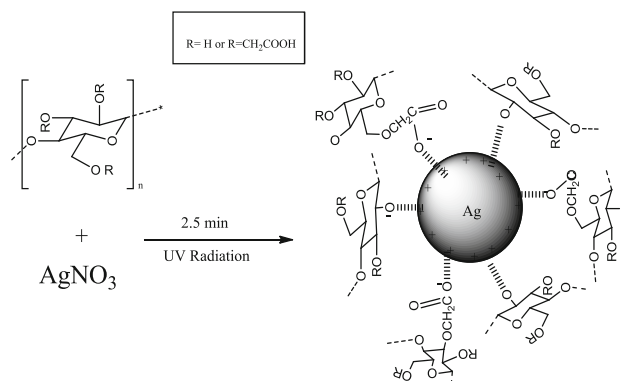
1 Introduction

In recent years, the term metal nanoparticles has arisen and metal nanoparticles have attracted great attention due to their large surface area to volume ratio as well as their unique optical, electronic, and catalytic properties, which make them find applications in many different fields [1, 2]. Metal nanoparticles are mainly utilized in many applications such as water purification, catalysis of chemical reactions, and hydrogen storage. For example, a wide range of applications have been found for metal nanoparticles in catalysis [3, 4], electronics [5], sensors and high-density information storage [6], photonics [7], pharmaceuticals, biotechnology, and medicine [8].

✉ Tarek M. Salama
  tm_salama@yahoo.com

[1] Department of Chemistry, Faculty of Science, Al-Azhar University, Nasr City, Cairo 11884, Egypt

[2] Forgery and Counterfeiting Researches Department, Forensic Medicine Authority, Ministry of Justice, Cairo, Egypt

Due to their high active surface area, metal nanoparticles generally tend to agglomerate forming larger particles. To prevent this agglomeration action and to stabilize and control the nanoparticles structures, various biological templates, synthetic polymers, natural polymers, and surfactants have been used [9–11]. Some biological systems have natural complicated mesoscopic and macroscopic structures with tremendous control over the placement of nanoscopic building blocks within extended architectures [12]. Thus, the use of organic polymers as templates can be considered as one of the most powerful and effective methods used to synthesize metal nanoparticles [13–15]. In addition to producing stable and dispersed nanoparticles with controlled size, shape, and distribution, this method also enables one to combine the desired properties of the template polymers together with the novel properties of the metal nanoparticles, which make the resulting composite suitable for different unique applications [16, 17].

Recently, much effort is focused on the biomimetic self-assembly of natural polymers. The concept of green synthesis of nanoparticles was first promoted by Raveendran et al. [18] in which glucose acted as reducing agent and starch played the role of particles stabilizer. Particularly, using natural polymers such as polysaccharides as templates for the preparation of metal nanoparticles has attracted much interest because the composites which are composed of natural polymers and metal nanoparticles provide great potential for biomedical applications such as in biosensing, therapy, bioimaging, and cancer therapy.

Silver has been used for its antimicrobial properties since ancient times [19]. When penicillin was discovered and the era of the antibiotics began, the use of silver for its antimicrobial properties decreased [20]. Since biocide-resistant strains have emerged, the interest in using silver as an antimicrobial agent has risen again [21]. However, antimicrobial agents based on ionic silver (e.g., silver nitrate) have one major drawback: They are easily inactivated by complexation and precipitation and thus have a limited usefulness [22]. Zerovalent silver nanoparticles were considered as a valuable alternative for ionic silver. It has been cited that silver nanoparticles are antimicrobial toward a broad spectrum of Gram-negative and Gram-positive bacteria [23, 24]. Furthermore, silver nanoparticles show antifungal [25] and antiviral activity [26, 27]. Besides their antimicrobial properties, silver nanoparticles can be used for their catalytic, conductive, and optical features [28–30]. Silver nanoparticles were prepared by means of using the carbohydrate polymer and sodium carboxymethyl cellulose. In that case, sodium carboxymethyl cellulose was found to work effectively as both reducing and stabilizing agents [2, 31].

The aim of the present study is to investigate carboxymethyl cellulose (CMC) as a stabilizing agent for the green synthesis of silver nanoparticles under UV photoirradiation. Studying the multiple reaction conditions including Ag^+ ion and CMC concentrations, UV exposure duration has been disclosed. The structural properties of the Ag nanoparticles embedded in CMC (AgNPs/CMC) produced as well as the influence of the interaction between CMC chains and Ag^+ while being reduced under UV irradiation was investigated. Thus, transmission electron microscopy (TEM), X-ray photoelectron spectroscopy (XPS), powder X-ray diffraction (XRD), Fourier transform infrared spectroscopy (FTIR), and UV–Visible spectroscopy tools were combined to characterize the obtained AgNPs/CMC. Finally, the silver nanoparticles were tested for antimicrobial activity.

2 Experimental

2.1 Synthesis of AgNPs/CMC

A simple one-step reaction of AgNO₃ (Merck) with CMC molecules (S. D. Fine Chem. Ltd., India, high viscosity, 98 %) was used to synthesize AgNPs embedded in CMC substrate. No other additives were used either to promote the reaction or to protect growth Ag particles. A stock solution of 0.1 M AgNO₃ solution was made and kept in the dark for the protection against sunlight. Then, 10 ml AgNO₃ solution was added drop by drop into an aqueous CMC solution (0.1 g dissolved in 200 ml distilled water at 50 °C for 30 min) while stirring at room temperature. The color of the mixed solution did change to confirm the existence of charged Ag^+. Afterward, the evaporated water is carried off at 80 °C under purging of nitrogen gas, and this sample is designated as Ag/CMC-air.

2.2 Preparation of Ag/CMC using UV photoirradiation

At 50 °C for 30 min with stirring, 0.1 g CMC was dissolved in 200 ml (0.5 g l⁻¹) distilled water and then cooled down to the room temperature, and then, 10 ml silver nitrate (0.1 M) solution was added drop wise to the CMC solution to finally give 5.0 mM. The resulting solution mixture was then subjected to UV irradiation under N₂ atmosphere at different times, i.e., 0.5, 1.0, 1.5, 2.0, 2.5, and 3.0 min. The UV light was generated in the high-pressure mercury lamp, 6 W at 245 nm. The cell used was made of quartz: 40 mm diameter and 195 mm height. The color of the resulting solution turns gradually to gray after 1.0 min, and therefore the Ag nanoparticles were obtained. Aliquots were then measured at 300–500 nm to ascertain the formation of silver nanoparticles. After finishing the reaction, an appropriate cut-off filter was placed in front of the reactor to remove the portion of the UV radiation. The samples were dried at 80 °C under N₂ gas; these samples were designated

as xAgNPs/CMC ($x = 0.5$–3.0), and the sample name prefix is related to the UV exposure time in min.

2.3 Effect of CMC concentration on the prepared Ag/CMC

Definite amounts of CMC 0.025, 0.05, 0.075, and 0.1 g in 200 ml distilled water were heated to 50 °C for 30 min. The turbid solution thus formed was cooled down to the room temperature in which a clear solution was obtained. Following this, 10 ml silver nitrate solution (0.1 M) was added drop wise to the CMC solution. The mixture solution samples were then UV-irradiated under N_2 gas at different time intervals.

2.4 Effect of AgNO₃ concentration

Certain volumes of solution with a certain molar concentration of silver nitrate (2–12 ml, 0.1 M) were added drop wise to 200 ml CMC solution (0.5 g l^{-1}) and then subjected to UV irradiation under N_2 gas at different time intervals. Different aliquots were then taken and checked by UV spectra for the production of silver nanoparticles.

2.5 Antimicrobial screening

The antibacterial activity of Ag nanoparticles stabilized into CMC matrix was tested against two types of bacteria: (1) Gram-negative bacteria: *Escherichia coli* NCTC 10416, *Pseudomonas aeruginosa* NCIB 9016 and (2) Gram-positive bacteria: *Bacillus subtilis* NCIB 3610, *Staphylococcus aureus* NCTC 7447, and fungi, namely *Candida albicans* IMRU 3669 using nutrient agar medium. The sterilized medium, autoclaved at 120 °C for 30 min at 40–50 °C, was incubated (1 ml/100 ml of medium) with the suspension (105 cfu ml^{-1}) of the microorganism (matched to McFarland barium sulfate standard) and poured into a petri dish to give a depth of 3–4 mm. The paper impregnated with the test compounds (μg/ml^{-1} in methanol) was placed on the solidified medium. The plates were pre-incubated for 1 h at room temperature and incubated at 37 °C for 24 and 48 h for antibacterial and antifungal activities, respectively. Ampicillin (mg/disk) was used as standard for antibacterial and antifungal activities. The observed zone of inhibition is presented in Fig. 10.

2.6 Physicochemical characterization

X-ray diffraction (XRD) data of the samples were measured at room temperature by using a Philips diffractometer (type PW 3710). The patterns were run with Ni-filtered copper radiation ($\lambda = 1.5404$ Å) at 30 kV and 10 mA with a scanning speed of $2\theta = 2.5°$/min.

The FTIR spectra were recorded on a Perkin-Elmer spectrometer (RXI FTIR) system, single beam with a resolution of 2 cm^{-1}. The samples were ground with KBr (1:100) as a tablet and mounted to the sample holder in the cavity of the spectrometer. The measurements were recorded at room temperature in the region 4000–400 cm^{-1}.

The size, morphology, and surface topology of the synthesized Ag particles on CMC solution were studied with transmission electron microscope (TEM) using a JEOL-JEM 1010 electron microscope films after ultramicrotoming with Leica EM UC6 ultramicrotome. The samples were prepared by placing a drop of the corresponding Ag nanoparticles solution onto a carbon-coated Cu grid followed by slow evaporation of solvent at ambient conditions.

X-ray photoelectron spectroscopy (XPS) measurements were obtained on a KRATOSAXIS 165 instrument equipped with dual aluminum–magnesium anodes using MgK$_\alpha$ radiation as the X-ray source at a power of 150 W (accelerating voltage 12 kV, current 6 mA) in a vacuum of 8.0×10^{-8} mPa. The measured samples were prepared by adding silver powder on freshly cleaved HOPG and drying at the room temperature.

The optical characterization of Ag colloids in water and AgNPs/CMC nanocomposite films was done using a Perkin-Elmer Lambda 35 spectrophotometer, employed at the range of 190–900 nm with the resolution of 0.5 nm.

3 Results and discussion

3.1 The UV–Vis spectroscopy

The effect of the following variables on the one-pot photoinduced synthesis of silver nanoparticles was investigated under normal laboratory conditions following three different experimental protocols. This includes (1) varying the length of UV exposure at fixed concentrations of CMC and AgNO₃, (2) varying concentration of CMC at fixed concentration of AgNO₃ and fixed length of UV exposure, and

Table 1 Antibacterial activity of synthesized Ag/CMC nanoparticles

Sample code	Test organism					
	Bacillus subtillus	*E. coli*	*Staphylococcus aureus*	*Pseudomonas aeruginosa*	*Candida albicans*	*A. niger*
Pure CMC	–	–	–	–	–	–
2.5 Ag/CMC	13.5	14	11	16	16	–

(3) varying concentration of AgNO₃ at fixed concentration of CMC and fixed length of UV exposure.

3.1.1 Effect of UV exposure time

The first experiment was conducted to determine the optimum length of UV exposure by exposing a mixed solution of AgNO₃ (5.0 mM) and CMC (0.5 g l^{-1}) to UV light for 0.5–3.0 min in order to obtain silver nanoparticles embedded in the CMC matrix (Fig. 1). A combination of UV and pure CMC only yielded a minimum absorption band at 256 nm (Fig. 1a), which may be assigned to a $\pi \rightarrow \pi^*$ transition derived from carbonyl groups (C=O) or ethylene unsaturated bonds (=C=C=) of the type (–CH=CH–)CO in the CMC structure [32, 33]. Likewise, the absorption spectrum of Ag$^+$/CMC without involving UV light exposure showed a blue shift in wavelength from 256 to 242 nm, and the absorbance value decreased (Fig. 1b). This is probably due to the interaction of CMC with Ag$^+$ ions, although plasmon absorption of nanosilver did not produce [34, 35]. Subsequent exposure to UV irradiation for 0.5 min brought about a weak broad band at

426 nm. As a result of gradual increase in UV exposure time from 0.5 to 2.5 min, the Ag$^+$/CMC solution evenly and gradually gets darker in color through concurrent formation of the silver nanoparticles. Concurrently, broad absorption bands from 350 to 550 nm with maxima at 403 nm were developed with UV irradiation time which can be a result of a surface plasmon resonance (SPR) phenomenon [36–39], as due to the formation of Ag nanoparticles (Fig. 1c–h). This observation is accompanied by a regular blue shift in the range of 426–403 nm. The blue shift is indicative of the formation of smaller silver nanostructures according to increase in reducing efficiency of Ag$^+$ ions to metallic Ag afforded by the photoactivated CMC [40]. Thus, 2.5 min of UV exposure was determined to be the optimum length of time for production small size of silver nanoparticles in CMC (2.5 AgNPs/CMC). The CMC fiber chains thus provide a more effective steric stabilization and reduce the crystal growth of the silver nanoparticles. Besides, the added CMC, alongside the stabilizing effect, accelerates the photocatalytic reduction of the Ag$^+$ ions.

3.1.2 Effect of CMC concentration

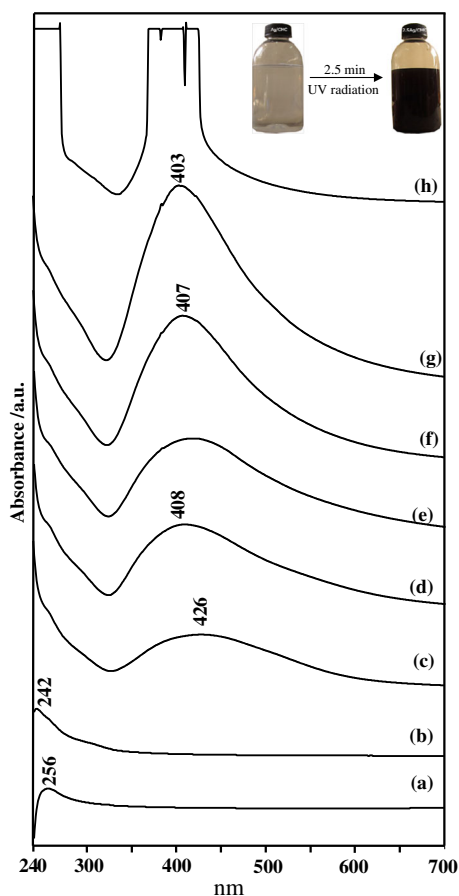To determine the optimum concentration of CMC providing a homogeneous state of reaction mixture in the reactor,

Fig. 1 UV–Vis spectra of AgNPs/CMC prepared at different times of UV exposure: (*a*) pure CMC, (*b*) 0.0 min, (*c*) 0.5 min, (*d*) 1.0 min, (*e*) 1.5 min, (*f*) 2.0 min, (*g*) 2.5 min, and (*h*) 3 min
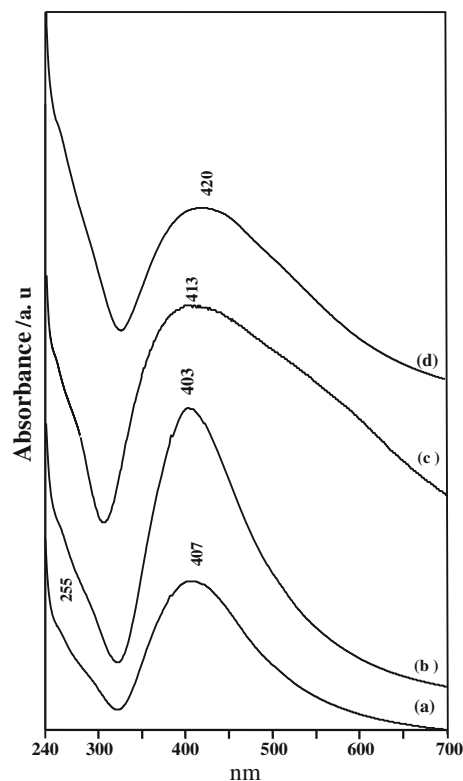
Fig. 2 UV–Vis spectra of AgNPs/CMC prepared at different CMC concentrations: (*a*) 0.25 g l^{-1}, (*b*) 0.5 g l^{-1}, (*c*) 0.75 g l^{-1}, and (*d*) 0.1 g l^{-1}

Fig. 2 shows the absorption spectra of AgNPs/CMC using a constant concentration of $AgNO_3$ (5.0 mM) and different CMC concentrations (0.25–1.0 g l^{-1}) in combination with 2.5 min of UV exposure. The spectra reveal that almost similar plasmon bands were formed near a wavelength at 407–403 nm in low CMC concentrations, i.e., 0.25–0.50 g l^{-1}, of ideal bell-shape characteristic for the formation of AgNPs. It is also clear that there is a gradual decrease in the absorption intensity of the 407–403 nm band by increasing the CMC concentration above 0.50 g l^{-1}, which might be ascribed to the CMC matrix-induced significant changes to AgNPs. Therefore, highly uniform silver nanoparticles would occur at optimal CMC concentration of 0.5 g l^{-1}. This figure also demonstrates another interesting influence of the CMC matrix on the spectra at higher concentrations of CMC, i.e., 0.5–1.0 g l^{-1}, where the plasmon bands experienced broadening and red shifting to longer wavelengths (Fig. 2c, d). Kreibig and Vollmer [41] have attributed this observation to concentrated colloids of silver nanoparticles which, in turn, result in agglomeration spread over in the aqueous solution. Thus, higher CMC concentrations brought about a faster photochemical reaction.

3.1.3 Effect of silver nitrate concentration

Figure 3 shows the UV–Vis spectra for AgNPs/CMC produced with $AgNO_3$ concentrations varying between 1.0
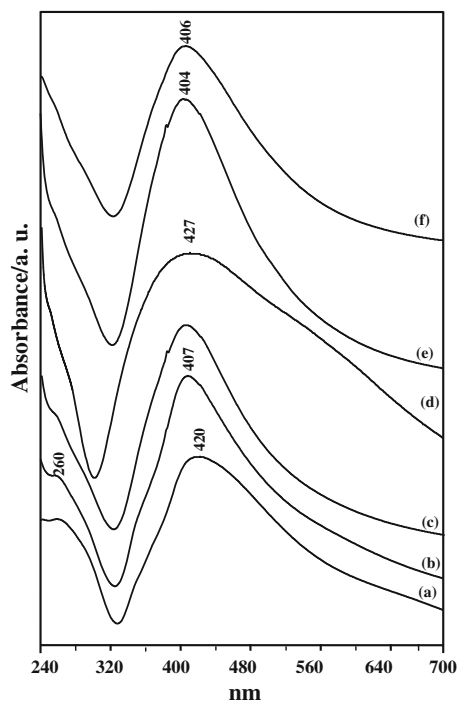

Fig. 3 UV–Vis spectra of AgNPs/CMC prepared at different concentrations of $AgNO_3$: (a) 1.0 mM, (b) 2.0 mM, (c) 3.0 mM, (d) 4.0 mM, (e) 5.0 mM, and (f) 6.0 mM

and 6.0 mM, a constancy of CMC concentration at 0.5 g l^{-1} and UV exposure time of 2.5 min. Similar absorption spectra were obtained at wavelength 420 nm, and the peaks intensity increases with increasing $AgNO_3$ concentration and shifted gradually to lower wavelength, i.e., 404 nm. This result is associated with a very tiny band at 260 nm delivered at lower concentrations of $AgNO_3$ (1.0–3.0 mM), indicating the presence of small amounts of Ag^+ in AgNPs/CMC [42, 43]. This band disappeared in favor of the band at 406 nm by increasing the concentration of $AgNO_3$ to 5.0 mM. Thus, the increase in Ag^+ concentration than 3.0 mM results in the formation of more AgNPs as evident by the increase in absorbance at 404 nm. In other words, in order to achieve better stability and efficient reduction for conversion of Ag^+ ions to silver nanoparticles with extremely small sizes, certain ratio of silver nitrate to CMC in the reaction medium must be ascertained. Consequently, an optimized concentration of $AgNO_3$ (5.0 mM) and CMC (0.5 g l^{-1}) at UV exposure time of 2.5 min was found to be best for complete photoinduced reduction of Ag^+ ions in the absence of any external reducing agents to get AgNPs/CMC composite. This sample is referred to as the 2.5 AgNPs/CMC.

3.2 X-ray diffraction (XRD) analysis

Figure 4 is the X-ray diffraction patterns of pure CMC before and after UV irradiation for 2.5 min, and AgNPs/CMC samples made with different CMC concentrations varying from 0.25 to 1.0 g l^{-1}, while the concentration of $AgNO_3$ was kept constant at 5.0 mM. The pure CMC showed one main peak at a (d) value of 4.31 Å, related to crystallinity of cellulose fibers [44] (Fig. 4a). Control UV light-irradiated CMC sample for 2.5 min had "halo" pattern characteristic of amorphous materials (Fig. 4b). This result suggests decrease in the lattice defects within the crystalline phase of CMC by the exposure to UV light [45, 46]. We arrived at the same conclusion by FTIR as shown below.

At low CMC concentration as 0.25 g l^{-1}, the XRD pattern showed diffraction peaks at (d) = 3.05 and 2.69 Å related to unreacted $AgNO_3$ precursor and other peaks at 2.36, 2.04, 1.44 and 1.23 Å related to face-centered cubic silver nanoparticles [42, 43, 47] (Fig. 4c). Increasing the CMC concentration to 0.05 g l^{-1} showed the trend of increasing intensity of these peaks on account of those related to unreacted $AgNO_3$, emphasizing the beneficial effect of CMC in the stabilizing of a distinct phase of face-centered cubic structure of AgNPs (Fig. 4d). Further increase in the CMC concentration to 1.0 g l^{-1} led to a dramatic decrease in intensity of the AgNPs XRD peaks (Fig. 4e), probably induced by the increased viscosity contributed significantly to hydrogen bonding of adjacent CMC molecules in the reaction solution.
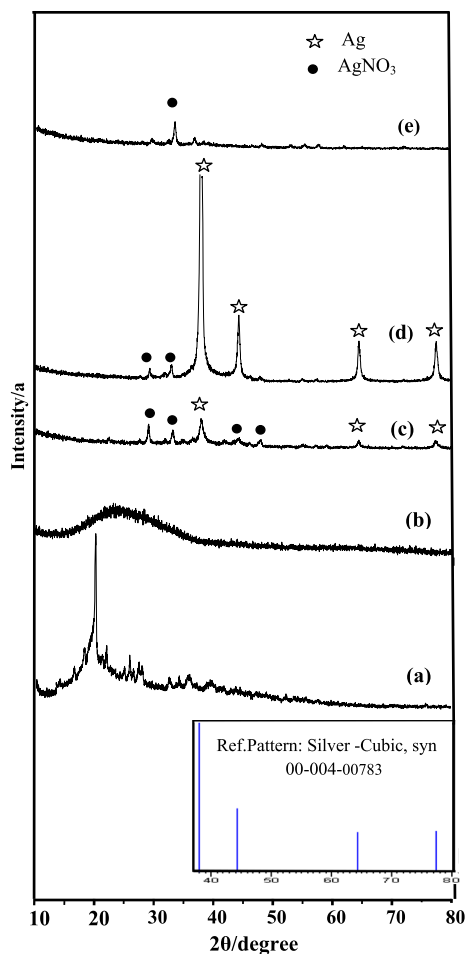
Fig. 4 XRD patterns of AgNPs/CMC prepared at different CMC concentrations: (a) pure CMC, (b) CMC after irradiation with UV for 2.5 min, (c) 0.25 g l⁻¹, (d) 0.5 % g l⁻¹, (e) 1.0 g l⁻¹

Figure 5 shows time-dependent effect of UV irradiation in the synthesis of crystalline AgNPs/CMC which is formed by the reaction of $AgNO_3$ (5.0 mM) over CMC (1.0 g l⁻¹). Short-time (1.0 and 1.5 min) exposure to UV radiation causes reflections of $AgNO_3$ at $(d) = 3.06$ and 2.68 Å, and a reflection of cubic structure of silver nanoparticles at 2.36 Å corresponds to (111) plane. Increasing UV exposure time to 2.5 min led to lines at d values of 2.36, 2.05, 1.45, and 1.23 Å and corresponded to (111), (200), (220), and (311) lattice planes of cubic crystalline structure of AgNPs, respectively, where they compared with the standard powder diffraction card of JCPDS file number 01-1167. The peak intensity of the (111) plane at $(d) = 2.36$ Å is very high, and this is due to the preferential adsorption of Ag atoms on that plane in the course of photochemical preparation of Ag nanoparticles. The average size of silver nanoparticles as estimated from the FWHM of the (111) and (200) planes of silver using the Debye–Scherrer formula was 4.4 nm. UV light is absorbed by molecules of CMC, and the photodissociative excitation
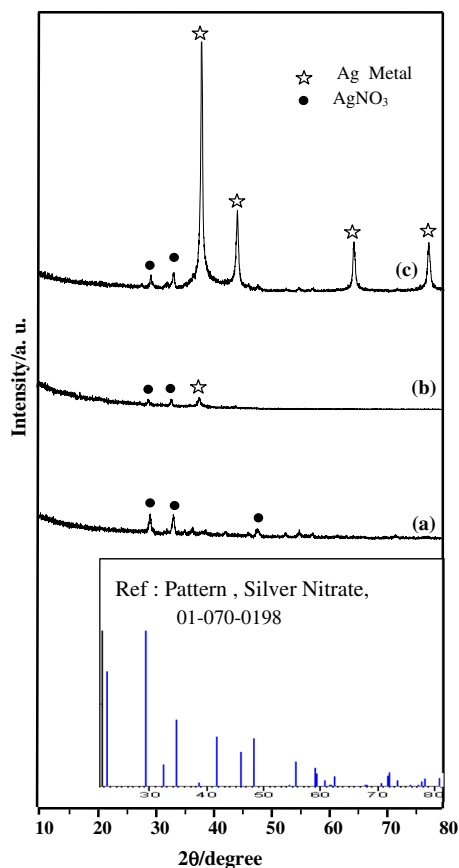

Fig. 5 XRD patterns of AgNPs/CMC prepared at different times of UV exposure: (a) 1.0 min, (b) 1.5 min, and (c) 2.5 min

of functional groups of CMC such as –COOH/–OH by photons will reduce Ag⁺ ions to Ag nanoparticles. These results are in good accordance with the literature [48]. This technique may provide the fastest yet method of preparing Ag nanoparticles in the CMC matrix.

3.3 XPS analysis

X-ray photoelectron spectroscopy (XPS) measurements were carried out to confirm the chemical state(s) of silver in the 2.5 AgNPs/CMC composite. Hence, the binding energy of Ag 3d is very sensitive to the chemical environment of Ag, which makes it a particularly suitable to probe the electron-donating ability of the polymeric CMC. Figure 6 shows the XPS spectrum of 2.5 AgNPs/CMC prepared through the reaction between CMC (0.5 g l⁻¹) and $AgNO_3$ (5 mM) in a total volume of 200 ml H_2O under UV radiation for 2.5 min. The survey spectrum of this sample showed characteristic peaks of O 1s at 533.91 eV, C 1s at 286.49 eV, and N 1s at 400.36 eV. The curve-fitting analysis of Ag^0 showed two intense peaks which appear at binding energies of 372.98 eV for Ag 3d3/2 and 379.11 eV for Ag 3d5/2 with 6.13 eV separations. Therefore, it is
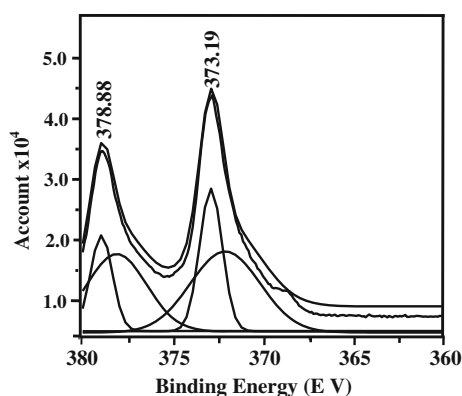
Fig. 6 Curve-fitted XPS spectra of 2.5 AgNPs/CMC prepared by exposing a mixed solution of 0.5 g l^{-1} CMC and 5.0 mM AgNO$_3$ in 200 ml distilled water to UV radiation for 2.5 min

clearly evident that Ag$^+$ ions are reduced to silver nanoparticles in the presence of CMC and UV light. In the survey spectrum, we did not observe peaks for the oxide formation, which indicates the stability of AgNPs. The O 1s peak is likely a consequence of surface oxygen atoms in CMC which remain attached to the AgNPs.

3.4 FTIR spectra

The FTIR spectra of the pure CMC before and after UV irradiation for 2.5 min and 2.5 AgNPs/CMC samples were used to obtain information about the surface interaction of CMC to the Ag(I) ions, and the results are displayed in Fig. 7. According to Pecsok et al. [49], carboxyl groups show two peaks at the wave numbers about 1600–1640 and 1400–1450 cm^{-1}. Therefore, the IR spectrum of CMC before irradiation exhibited two characteristic absorption bands at 1622 and 1432 cm^{-1} assigned to v_{as}(COO$^-$) and v_s(COO$^-$) carboxylate vibrational stretching, respectively (Fig. 7a). The crystallinity index of irradiated CMC was decreased due to breaking of some hydrogen bonds in the crystalline parts of cellulose chains [50], which was confirmed by decreasing the intensity of the main hydroxyl group at 3410 cm^{-1} as well as its shift to 3432 cm^{-1} (Fig. 7b). The decrease in crystallinity of CMC after irradiation was also indicated by vanishing of the 3356 and 3316 cm^{-1} bands of an extensive hydrogen bonding. These observations are on the whole consistent with the loss in crystalline order observed via XRD of irradiated CMC.

The downward shift of the v_{as}(COO$^-$) stretching band from 1622 to 1605 cm^{-1} as well as vanishing of the v_s(COO$^-$) band in the spectrum of 2.5 AgNPs/CMC (Fig. 7c) suggests coordination of the –COO$^-$ groups to Ag$^+$ ions. Interestingly, an IR peak at around 1371 cm^{-1} that corresponds to the symmetric stretching mode of carboxylate
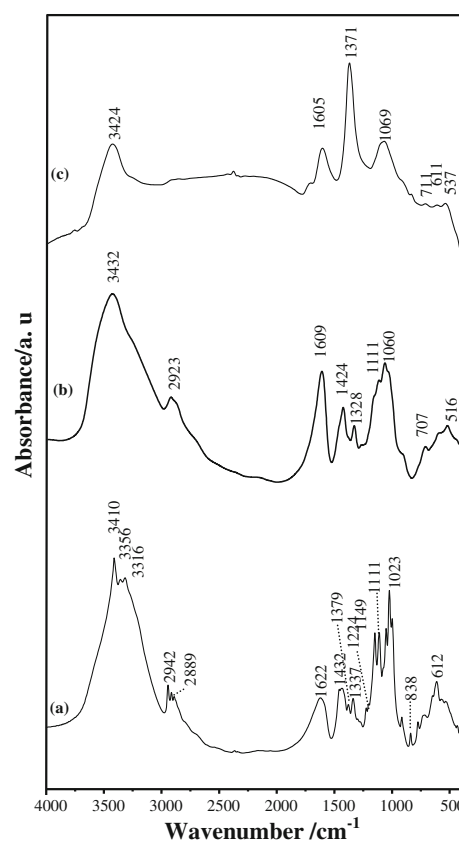

Fig. 7 FTIR spectra for (*a*) pure CMC, (*b*) CMC after irradiation with UV for 2.5 min, and (*c*) 2.5 AgNPs/CMC

(COO$^-$) groups has grown very strong in the spectrum of 2.5 AgNPs/CMC, which is considered to be a characteristic of carboxylic acids adsorbed on AgNPs [51]. It has been reported that the changes related to carboxylate stretching bands might indicate mode of Ag$^+$ interaction with –COO$^-$ groups in CMC from the wavenumber separation, Δv, between the v_{as}(COO$^-$) and v_s(COO$^-$) bands. The values of $\Delta v = v_{as}$(COO)$-v_s$(COO) in monodentate complexes are expected to be much larger than 350 cm^{-1}, and the smallest Δv (<200 cm^{-1}) is for the chelating bidentate interaction. When $200 < \Delta v < 350$ cm^{-1}, the carboxylate group is present as an intermediate state between monodentate and bidentate, which is called anisobidentate. In our work, the Δv value is 226 cm^{-1} (1605–1379 cm^{-1}); thus, anisobidentate carboxylate on isolated Ag(I) sites could belong to the interaction mode. Ag(I) carboxylates mostly form bridged dimers (Ag$_2$L$_2$) and also polymeric network [52].

In a study characterizing CMC, peaks at 3410, 3356, and 3316 cm^{-1} were allocated to free OH stretching vibration and inter- and intra-molecular hydrogen bonds, respectively [53]. It is clear that the crystallinity of CMC was further decreased after completion of the reaction and stabilizing AgNPs in CMC (Fig. 7c). This can be
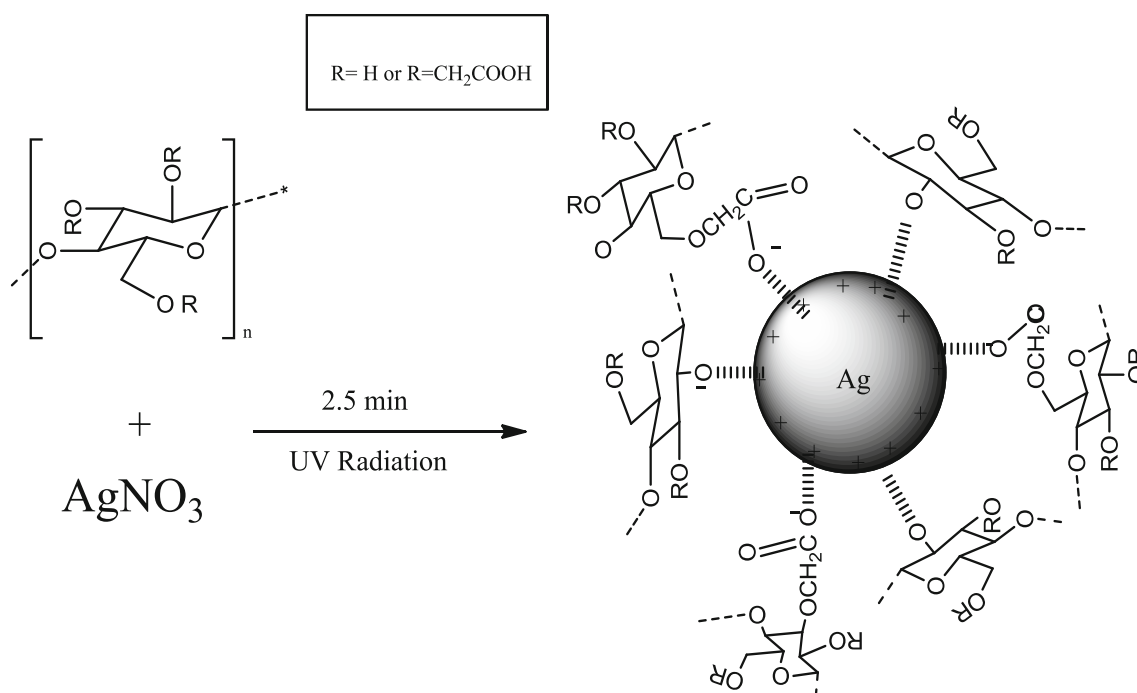
Fig. 8 Proposed schematic diagrams for the interaction of $AgNO_3$ with CMC under UV radiation for 2.5 min

confirmed by the band at 3410 cm^{-1} that experienced a decrease in intensity as well as a downward shift from 3432 to 3424 cm^{-1}. This is consistent with the decrease in the hydrogen bonds in the crystalline part of the cellulose chain, which could be interpreted as due to the polarization of the cellulose O–H and carboxymethylic (–CH$_2$–COOH) groups. The photochemical reactions in the 2.5 AgNPs/CMC composite is initiated by one-electron transfer from the hydroxyl/carboxylate ion to the bound Ag$^+$ ion, giving rise to silver atoms (Fig. 8). The carboxyl radical (RCOO$^{\cdot}$) is converted to carboxylic acid (RCOOH) as a result of hydrogen abstraction from the C–H bond of the polymer chain. This is manifested by the dramatic increase in band intensity at 1371 cm^{-1} characteristic of adsorbed carboxylic acid (Fig. 7c).

Another change in the IR spectrum of the 2.5 AgNPs/CMC was observed for the band at 1023 cm^{-1}, which occurs as a result of the C–O–C glycosidic ether links [54]. This band completely disappeared owing to ether bond cleavage after the introduction of Ag$^+$ in the CMC structure. Thus, more highly anionic CMC would be expected to interact more strongly with Ag$^+$ ions through not only negatively charged COO$^-$ groups but also ionized OH$^-$ groups too. The large number of these anions on CMC can facilitate the reduction of Ag$^+$ ions to AgNPs when exposed to UV light. Very likely Ag$^+$ interacts weakly with OH$^-$ derived from dissociated H$_2$O molecules to produce a very weak feature at 3754 cm^{-1} due to Ag-OH. However, the same was not observed for the undoped CMC sample.
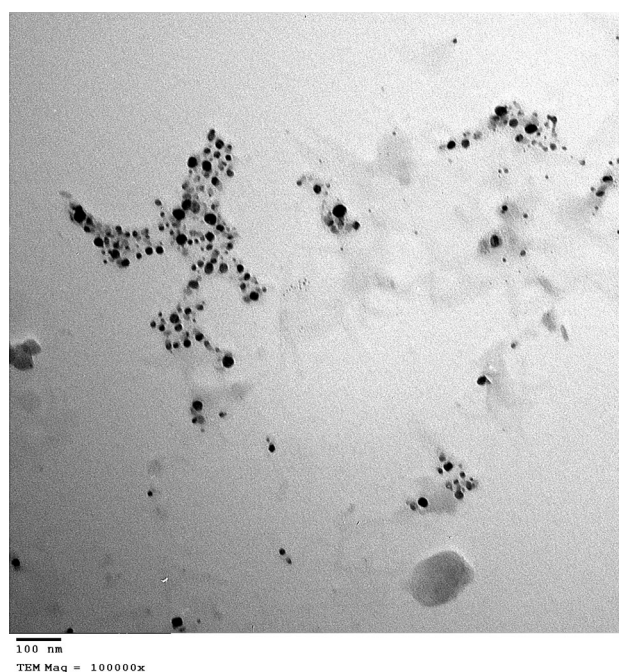

100 nm
TEM Mag = 100000x

Fig. 9 TEM image of the 2.5 AgNPs/CMC sample

3.5 Transmission electron microscopy (TEM) analysis

Figure 9 shows the TEM image of the 2.5 AgNPs/CMC sample, which shows typical spherical Ag nanoparticles

within the polymeric matrix. The nanoparticles were separated from each other, and sizes of the primary AgNPs particles varying between 2 and 15 nm were determined. The TEM image of this sample also indicated that the particles are well dispersed in the solution. Thus, the UV–Vis spectra supported by the XRD, XPS, and TEM indicated that CMC is an effective reducing agent for Ag salt to produce AgNPs with higher degree of monodispersion under UV irradiation.

3.6 Biological activity

The investigated 2.5 AgNPs/CMC and pure CMC were tested against antibacterial activity in vitro using the paper disk diffusion technique [55, 56]. The tested microorganism strains were: Gram-negative bacteria: *E. coli* NCTC 10416, *P. aeruginosa* NCIB 9016 and Gram-positive bacteria: *B. subtilis* NCIB 3610, *S. aureus* NCTC 7447; the results of antimicrobial activity values and zone of inhibition are given in Fig. 10 and Table 1. From Table 1, it has been clarified that CMC was inactive toward all Gram-positive and Gram-negative bacteria, whereas 2.5 AgNPs/CMC exhibited moderate activity against *B. subtilis* and *E. coli* bacteria when compared to the inhibitory activity toward *P. aeruginosa* and *C. albicans*. In the contrary, 2.5 AgNPs/CMC showed a loss in activity against *S. aureus*, but the remaining members exhibited weak activity. A lower value exhibited by the silver nanoparticles against *S.*

aureus is of great significance in the healthcare delivery system. The silver nanoparticles could be used as an alternative to orthodox antibiotics in the treatment of infections caused by the microorganisms, especially because they frequently develop resistance to known antibiotics. The less pronounced effect on *S. aureus* compared with *P. aeruginosa* is probably due to the different cell wall structure of Gram-positive and Gram-negative bacteria. Gram-negative *P. aeruginosa* is more sensitive to silver than Gram-positive *S. aureus*. Based on these results, the obtained hybrid materials with Ag nanoparticles have efficient antibacterial properties for both Gram-positive and Gram-negative bacteria. The antibacterial action of silver may be due to the interaction with the bacterial cell wall resulting in cell wall rupture, leading to protein denaturation and cell death. Silver and silver ions can cause oxidative stress by free radical formation in cytoplasm and disruption of bacterial membrane. Many authors [57] established that the action of silver nanoparticles is similar to that of silver ions. Yoon et al. [58] investigated the antibacterial activity of silver nanoparticles and reported that the *P. aeruginosa* is more sensitive to silver nanoparticles compared to *S. aureus*, due to different cell wall structure of Gram-positive and Gram-negative bacteria. Similar data were reported by Lara et al. [59] as a result of investigation of bactericidal effect of silver nanoparticles against multidrug-resistant bacteria. It is believed that DNA loses its replication ability and the cellular proteins
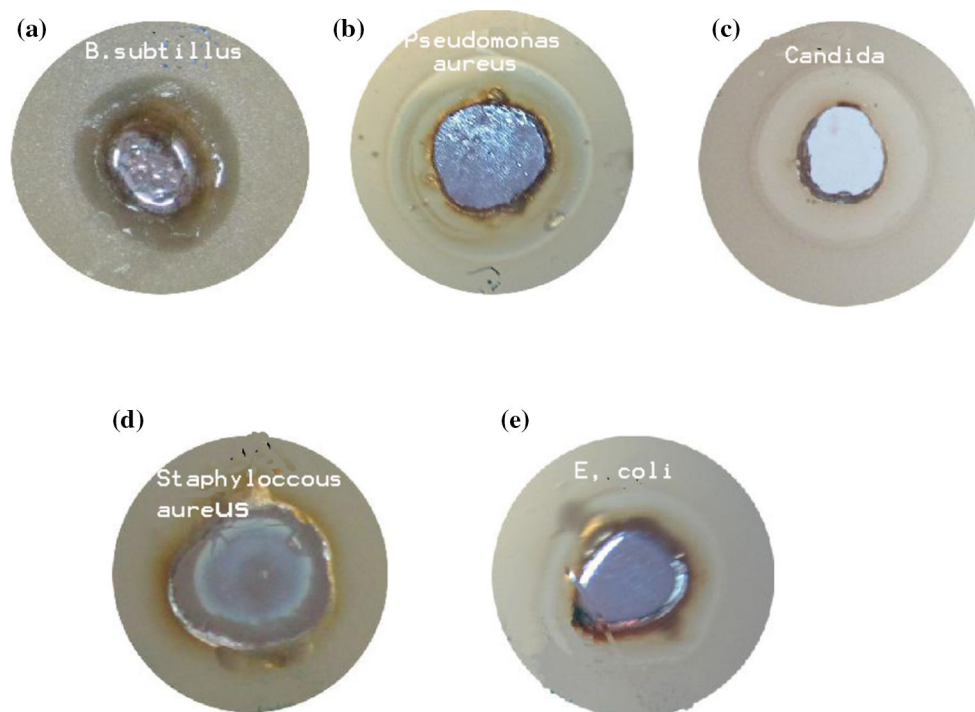

Fig. 10 Antimicrobial activity of 2.5 AgNPs/CMC for: **a** *B. subtillus*, **b** *Pseudomonas aeruginosa*, **c** candida, **d** *Staphylococcus aureus*, and **e** *E. coli*

become inactivated on Ag$^+$ treatment [60]. In addition, it was also shown that Ag$^+$ binds to functional groups of proteins, resulting in protein denaturation [61]. However, the Ag$^+$ ions have only limited usefulness as antimicrobial agents for several reasons: the interfering effects of salts and the discontinuous release of inadequate concentrations of Ag$^+$ ions from the metal. In contrast, these limitations can be overcome by using AgNPs because they are highly reactive species due to their large surface areas [62].

In vitro antifungal studies from 2.5 AgNPs/CMC and pure CMC were tested against *C. albicans* IMRU 3669, Aspergillus niger ferm-BAM C-21, and the antifungal activity is presented in Table 1. In general, all the AgNPs samples exerted more activation in vitro antifungal activity against the tested organism.

4 Conclusions

A green chemistry approach for the synthesis of AgNPs in the CMC matrix using aqueous solution of silver nitrate under UV irradiation has been evidenced experimentally. CMC served as the reducing agent during the synthesis as well as stabilizing matrix for AgNPs in highly dispersed fashion. The fabrication procedure of the AgNPs was done by using well-defined experimental conditions including variation of the concentrations of silver nitrate and CMC and variation in the length of UV exposure. The outcome of these experiments demonstrates that the stability of Ag$^+$ toward reduction to AgNPs would increase at a very short UV irradiation below 3.0 min. The Ag$^+$ reduction mechanism was mainly dependent on the presence of the –COOH and –OH surface species in the fiber host matrix of CMC. Thus, the synthesis of AgNPs/CMC was efficient, straightforward, and did not need any harsh reduction conditions. The synthesized AgNPs were stable for more than a month under ambient conditions without the indication of oxide formation.

The interactions of positively and negatively charged AgNPs with bacterium *E. coli*. showed that positively charged AgNPs deposited better with the bacteria surface compared with the negatively charged ones. The present research could find new applications for a fast synthesis process of other nanomaterials as well as to understand the interactions of AgNPs with microorganisms.

References

1. Babu VR, Kim C, Kim S, Ahn C, Lee Y (2010) Development of semi-interpenetrating carbohydrate polymeric hydrogels embedded silver nanoparticles and its facile studies on *E. coli*. Carbohydr Polym 81:196–202

2. Hebeish AA, El-Rafie MH, Abdel-Mohdy FA, Abdel-Halim ES, Emam HE (2010) Carboxymethyl cellulose for green synthesis and stabilization of silver nanoparticles. Carbohydr Polym 82:933–941

3. Biffis A, Orlandi N, Corain B (2003) Microgel-stabilized metal nanoclusters: size control by microgel nanomorphology. Adv Mater 15:1551–1555

4. Daniel MC, Astrue D (2004) Gold nanoparticles: assembly, supramolecular chemistry, quantum-size-related properties, and applications toward biology, catalysis, and nanotechnology. Chem Rev 104:293–346

5. Kiesow A, Morris JE, Radehaus C, Heilmann A (2003) Switching behavior of plasma polymer films containing silver nanoparticles. J Appl Phys 94:6988–6990

6. Vaseashta A, Dimova-Malinovska D (2005) Nanostructured and nanoscale devices, sensors and detectors. Sci Technol Adv Mater 6:312–318

7. Xu S, Zhang J, Paquet C, Lin Y, Kumacheva E (2003) From hybrid microgels to photonic crystals. Adv Funct Mater 13:468–472

8. Xu ZP, Zeng QH, Lu GQ, Yu AB (2006) Inorganic nanoparticles as carriers for efficient cellular delivery. Chem Eng Sci 61:1027–1040

9. Bajpai SK, Mohan YM, Bajpai M, Tankhiwale R, Thomas V (2007) Synthesis of polymer stabilized silver and gold nanostructures. J Nanosci Nanotechnol 7:2994–3010

10. Esumi K, Suzuki A, Yamahira A, Torigoe K (2000) Role of poly (amidoamine) dendrimers for preparing nanoparticles of gold platinum and silver. Langmuir 16:2604–2608

11. Esumi K, Isono R, Yoshimura T (2004) Preparation of PAMAM- and PPI-metal (silver, platinum, and palladium) nanocomposites and their catalytic activities for reduction of 4-nitrophenol. Langmuir 20:237–243

12. Mandal S, Phadtare S, Sastry M (2005) Interfacing biology with nanoparticles. Curr Appl Phys 5:118–127

13. Božanić DK, Dimitrijević-Branković S, Bibić N, Luyt AS, Djoković V (2011) Silver nanoparticles encapsulated in glycogen biopolymer: morphology, optical and antimicrobial properties. Carbohydr Polym 83:883–890

14. Hang AT, Tae B, Park JS (2010) Non-woven mats of poly (vinyl alcohol)/chitosan blends containing silver nanoparticles: fabrication and characterization. Carbohydr Polym 82:472–479

15. Kora AJ, Sashidhar RB, Arunachalam J (2010) Gum kondagogu (Cochlospermum gossypium): a template for the green synthesis and stabilization of silver nanoparticles with antibacterial application. Carbohydr Polym 82:670–679

16. Du WL, Niu SS, Xu YL, Xu ZR, Fan CL (2009) Antibacterial activity of chitosan tripolyphosphate nanoparticles loaded with various metal ions. Carbohydr Polym 75:385–389

17. Maneerung T, Tokura S, Rujiravanit R (2008) Impregnation of silver nanoparticles into bacterial cellulose for antimicrobial wound dressing. Carbohydr Polym 72:43–51

18. Raveendran P, Fu J, Wallen SL (2003) Completely "green" synthesis and stabilization of metal nanoparticles. J Am Chem Soc 25:13940–13941

19. Silver S, Phung LT, Silver G (2006) Silver as biocides in burn and wound dressings and bacterial resistance to silver compounds. J Ind Microbiol Biotechnol 33:627–634

20. Klasen HJ (2000) Historical review of the use of silver in the treatment of burns. I. Early uses. Burns 26:117–130

21. Klasen HJ (2000) A historical review of the use of silver in the treatment of burns. II. Renewed interest for silver. Burns 26:131–138

22. Atiyeh BS, Costagliola M, Hayek SN, Dibo SA (2007) Effect of silver on burn wound infection control and healing: review of the literature. Burns 33:139–148

23. Kim JS, Kuk E, Yu KN, Kim JH, Park SJ, Lee HJ, Kim SH, Park YK, Park YH, Hwang CY, Kim YK, Lee YS, Jeong DH, Cho MH (2007) Antimicrobial effects of silver nanoparticles. Nanomedicine 3:95–101

24. Panacek A, Kvitek L, Prucek R, Kolar M, Vecerova R, Pizurova N, Sharma VK, Nevecna T, Zboril R (2006) Silver colloid nanoparticles: synthesis, characterization, and their antibacterial activity. J Phys Chem B 110:16248–16253

25. Kim KJ, Sung WS, Moon SK, Choi JS, Kim JG, Lee DG (2008) Antifungal effect of silver nanoparticles on dermatophytes. J Microbiol Biotechnol 18:1482–1884

26. Elechiguerra JL, Burt JL, Morones JR, Camacho-Bragado A, Gao X, Lara HH, Yacaman MJ (2005) Interaction of silver nanoparticles with HIV-1. J Nanobiotechnol 3:3–6

27. Lu L, Sun RWY, Chen R, Hui CK, Ho CM, Luk JM, Lau GKK, Che CM (2008) Silver nanoparticles inhibit hepatitis B virus replication. Antivir Ther 13:253–262

28. Medina F, Chimentao RJ, Kirm I, Rodriguez X, Cesteros Y, Salagre P, Sueiras JE, Fierro JLG (2005) Sensitivity of styrene oxidation reaction to the catalyst structure of silver nanoparticles. Appl Surf Sci 252:793–800

29. Fuller SB, Wilhelm EJ, Jacobson JA (2002) Monolithic micro-fabricated valves and pumps by multilayer soft lithography. J Microelectromech Syst 11:54–60

30. Kamat PV (2002) Photophysical, photochemical and photocatalytic aspects of metal nanoparticles. J Phys Chem B 106:7729–7744

31. Chen J, Wang J, Zhan X, Jin Y (2008) Microwave-assisted green synthesis of silver nanoparticles by carboxymethyl cellulose sodium and silver nitrate. Mater Chem Phys 108:421–424

32. Jayasekara R, Harding I, Bowater I, Christie GBY, Lonergan GT (2004) Preparation, surface modification and characterisation of solution cast starch PVA blended films. Polym Test 23:17

33. Whelan AM, Brennan ME, Blau WJ, Kelly JM (2004) Enhanced third-order optical nonlinearity of silver nanoparticles with a tunable surface plasmon resonance. J Nanosci Nanotechnol 4:66–68

34. Silvert P-Y, Herrera-Urbina R, Tekaia-Elhsissen K (1997) Preparation of col- loidal silver dispersions by polyol process. J Mater Chem 7:293–299

35. Aziz SB, Abidi ZHZ, Arof AK (2010) Influence of silver ion reduction on electrical modulus parameters of solid polymer electrolyte based on chitosan-silver triflate electrolyte membrane. Express Polym Lett 4:300–310

36. Itakura T, Torigoe K, Esumi K (1995) Preparation and characterization of ultrafine metal particles in ethanol by UV irradiation using a photoinitiator. Langmuir 11:41291

37. Foss CA, Hornyak GL, Stockert JA, Martin CR (1994) Template-synthesized nanoscopic gold particles: optical spectra and the effects of particle size and shape. J Phys Chem 98:2963–2971

38. Jana NR, Gearheart L, Murphy CJ (2001) Wet chemical synthesis of high aspect ratio cylindrical gold nanorods. J Phys Chem B 105:4065–5067

39. Othman IA (2013) Synthesis and characterization of Ag0/PVA nanoparticles viaphoto- and chemicalreduction methods for antibacterial study. Colloids Surf A 436:922–929

40. Li D, Komarneniw S (2006) J Am Ceram Soc 89:1510–1517

41. Kreibig U, Vollmer M (1995) Optical properties of metal clusters, vol 25. Springer, Berlin, p 535

42. Gautam A, Ram S (2010) Preparation and thermomechanical properties of Ag-PVA nanocomposite films. Mater Chem Phys 119:266–271

43. Ram S, Gautam A, Fecht HJ, Cai J, Bansmann H, Behm RJ (2007) A new allotrope structure of silver nanocrystals in anisotropic nucleation and growth in support over planar polymer molecules. Philos Mag Lett 87:361

44. Chai MN, Isa MIN (2013) The oleic acid composition effect on the carboxymethyl cellulose based biopolymer electrolyte. J Cryst Process Technol 28:31003

45. Chen CJ, Yeh GSY (1991) Radiation-induced crosslinking: III. Effect on the crystalline and amorphous density fluctuations of polyethylene. Colloid Polym Sci 269:353–363

46. Nawapat D, Thawien W (2013) Effect of UV-treatment on the properties of biodegradable rice starch films. Int Food Res J 20:1313–1322

47. X-Ray powder diffraction file JCPDS-ICDD (1999) Joint committee on powder diffraction standard-international centre for diffraction data. Swarthmore, PA, (a) 04-0783

48. Pouretedal HR, Norozi A, Keshavarz MH, Semnani A (2009) Nanoparticles of zinc sulfide doped with manganese, nickel and copper as nanophotocatalyst in the decolorization of organic dyes. J Hazard Mater 162:674–681

49. Pescok RL, Shields LD, Caims T, McWilliam IG (1976) Modern methods of chemical analysis. Wiley, New York

50. Wang J, Somasundaran P (2005) Adsorption and conformation of CMC at solid–liquid interfaces using spectroscopic, AFM and allied techniques. J Colloid Interface Sci 291:75–83

51. Donati I, Travan A, Pelillo C, Scarpa T, Coslovi A, Bonifacio A (2009) Polyol synthesis of silver nanoparticles: mechanism of reduction by alditol bearing polysaccharides. Biomacromolecules 10(2):210–213

52. Lancashire RJ (1987) In: Comprehensive coordination chemistry, vol. 54. Pergamon Press, Oxford

53. Pushpamalar V, Langford SJ, Ahmad M, Lim YY (2006) Optimization of reaction conditions for preparing carboxymethyl cellulose from sago waste. Carbohydr Polym 64:312–318

54. Mallapragada SK, Peppas NA (1996) Mechanism of dissolution of semi-crystalline poly(vinyl alcohol) in water. J Polym Sci B 34:1339–1346

55. Masquelin T, Obrecht D (2001) A new general three component solution-phase synthesis of 2-amino-1,3-thiazole and 2,4-di-amino-1,3-thiazole combinatorial libraries. Tetrahedron 57:153

56. Sah MM, Joshi PC (1989) Asian, synthesis and antifungal activity of some 2-arylimino-3-phthalimidoacetyl-4-thiazolidinones and their 5-arylidine derivatives. J Chem 1:141

57. Rastogi Sh, Rutledge V, Gibson Ch, Newcombe D, Branen J, Branen L (2011) Ag colloids and Ag clusters over EDAPTMS-coated silica nanoparticles: synthesis, characterization and antibacterial activity against *Escherichia coli*. Nanomed Nanotechnol Biol Med 7:305–314

58. Yoon K, Byeon JH, Park J, Hwang J (2007) Susceptibility constants of *Escherichia coli* and *Bacillus subtilis* to silver and copper nanoparticles. Sci Total Environ 373:572–575

59. Lara H, Ayala-Nunez N, Turrent L, Padilla CR (2010) Bactericidal effect of silver nanoparticles against multidrug-resistant bacteria. World J Microbiol Biotechnol 26:615–621

60. Feng QL, Wu J, Chen GQ, Cui FZ, Kim TM, Kim JO (2000) A mechanistic study of the antibacterial effect of silver ions on *Escherichia coli* and *Staphylococcus aureus*. J Biomed Mater Res 52:662–668

61. Spadaro JA, Berger TJ, Barranco SD, Chapin SE, Becker RO (1974) Antibacterial effects of silver electrodes with weak direct current. Microbial Agents Chemother 6:637–642

62. Nabikhan A, Kandasamy K, Raj A, Alikunhi NM (2010) Synthesis of antimicrobial silver nanoparticles by callus and leaf extracts from saltmarsh plant, Sesuvium portulacastrum L. Colloids Surf B 79(2):488–493